Supporting Information: Molecular Dynamics of Membrane-Spanning DNA Channels: Conductance Mechanism, Electro-Osmotic Transport and Mechanical Gating

Jejoong Yoo[†,‡] and Aleksei Aksimentiev[*,†,‡,¶]

†*Department of Physics, University of Illinois at Urbana–Champaign, 1110 West Green Street, Urbana, Illinois 61801*

‡*Center for the Physics of Living Cells*

¶*Beckman Institute for Advanced Science and Technology*

E-mail: aksiment@illinois.edu

Simulation methods

General MD protocols

All MD simulations were performed using the NAMD program,[1] periodic boundary conditions, CHARMM36 force field for DNA,[2] the TIP3P model of water,[3] and custom CHARMM-compatible parameters for ions.[4,5] Parameters for the charge-neutral nucleotides containing the ethyl-phosphate groups instead of phosphate groups were obtained using the CHARMM36 CGenFF.[6] Note that we employed ethyl-phosphate, not ethyl-phosphorothioate as in Ref. 7, due to the lack of reliable parameters for phosphorothioate. We expect that the difference is minor because the effect of backbone modifications on the structure and conductance of the channel results mainly from the ethyl groups, not the replacement of an oxygen atom with a sulfur atom in the DNA backbone. CHARMM-compatible model of diphytanoyl phosphatidylcholine (DPhPC) was taken from Ref. 8. The van der Waals and short-range electrostatic energies were calculated using an 8–10 Å switching scheme. The long-range electrostatic interactions were computed using the particle-mesh Ewald scheme and a grid of ∼1.2 Å.[9] The integration time step was 2 fs; 2–2–6 fs multiple timestepping was used.[1] Temperature was held constant at 298 K using a Langevin thermostat.[1] Pressure was maintained at 1 bar using the Nosé-Hoover Langevin piston pressure control.[10]

Preparation of the atomistic structure of DNA channel

We built the all-atom model of the DNA origami channel (System I)[7] utilizing our recently reported protocol.[5] First, we designed the path and the sequence (M13) of the DNA strands using the caDNAno program.[11] The path and sequence files were exported to JSON and CSV file formats, respectively, using caDNAno. Second, those caDNAno output files were converted to a PDB format structure file using our automated conversion program[5] maintained at the nanoHub web site.[12] Finally, the phosphate groups inside the transmembrane domain of the channel were covalently modified by adding ethyl groups to phosphate groups

using the IC command of the CHARMM program.[13]

Equilibration of the DNA channel in a lipid bilayer

The DNA origami channel was embedded in a pre-equilibrated system consisting of a DPhPC lipid bilayer and solvent, by placing the DNA origami channel in the lipid bilayer and removing overlapping lipid and water molecules. Following that, we created a 1 M solution of KCl by randomly replacing a number of water molecules with ions. The fully assembled system was energy-minimized for 5000 steps. After minimization, we performed 10 ns of equilibration having all non-hydrogen atoms of DNA harmonically restrained using the force constant $k = 0.5$ kcal/mol/Å^2, which allowed the lipid and solvent to equilibrate without affecting the structure of the DNA channel. During the equilibration, constant surface tension–constant temperature (NPγT) ensemble at zero surface tension ($\gamma = 0$) was used allowing the system to find its equilibrium dimensions. For the next 5 ns, the spring constant of the harmonic restraints was reduced to $k = 0.1$ kcal/mol/Å^2. After confirming that the DNA-lipid interface and the system's dimensions were stabilized, we performed an additional simulation for 55 ns at zero surface tension without applying any restraints. At the end of the equilibration simulation, the area per lipid was ∼88 Å^2, consistent with the experimental value.[8] The final system contained a DNA channel, 254 lipid molecules (127 per leaflet), 52,871 water molecules, 1,452 K^+, and 1,034 Cl^- ions in a rectangular box of ∼110×110×174 Å^3.

Preparation of compressed and stretched lipid bilayer systems

The system featuring a compressed lipid bilayer was made starting from the system equilibrated under zero surface tension. To reduce the area of the lipid bilayer, we performed an MD simulation under the NPγT ensemble at a surface tension of -100 dyn/cm using the SurfaceTensionTarget function of NAMD. During the simulation, the area and the height of the simulation system gradually decreased and increased, respectively. Within 50 ns, the system's dimensions changed from ∼110×110×174 Å^3 to ∼105×105×191 Å^3. In the compressed

bilayer system, the area per lipid was 77 Å^2. During the lipid compression simulation, we harmonically restrained the non-hydrogen atoms of DNA to the coordinates obtained at the end of the tension-free equilibration using the force constant of 1 kcal/mol/Å^2. After reaching the target area-per-lipid, we continued the simulation for another 40 ns in the constant area–constant temperature (NPAT) ensemble without applying any restraints to DNA.

The stretched lipid bilayer system (the lipid extension conditions) were made starting from the conformation observed at the end of the tension-free equilibration. To increase the area per lipid by about 15%, we randomly removed 20 lipid molecules from each bilayer leaflet. The system was then equilibrated for ∼50 ns under the NPAT ensemble having all non-hydrogen atoms of DNA restrained. Following this, the stretched bilayer system was equilibrated for additional ∼50 ns under NPAT without any restraints applied to DNA.

Calculation of the density-flow maps

We computed the streamline flow plots in the density-flow maps using the method described in Ref. 14. Using an MD trajectory sampled every 4.8 ps, we computed the three-dimensional flow vectors partitioning the simulation system into rectangular $\sim 2 \times 2 \times 2$ Å^2 blocks. Each of the 3D flow vectors was transformed to a cylindrical coordinate system that had the origin at the center of the transmembrane domains. By averaging the flow vectors in the cylindrical coordinate system over the azimuthal angle, we obtained the distribution of the flow vectors within the $r-z$ plane. Following that, the 2D flow vector field was made symmetric about the z axis by averaging over their mirror images ($r \to -r$). Finally, we obtained the streamline plots of the symmetrized 2D flow vector field using the streamline function of the python matplotlib package.

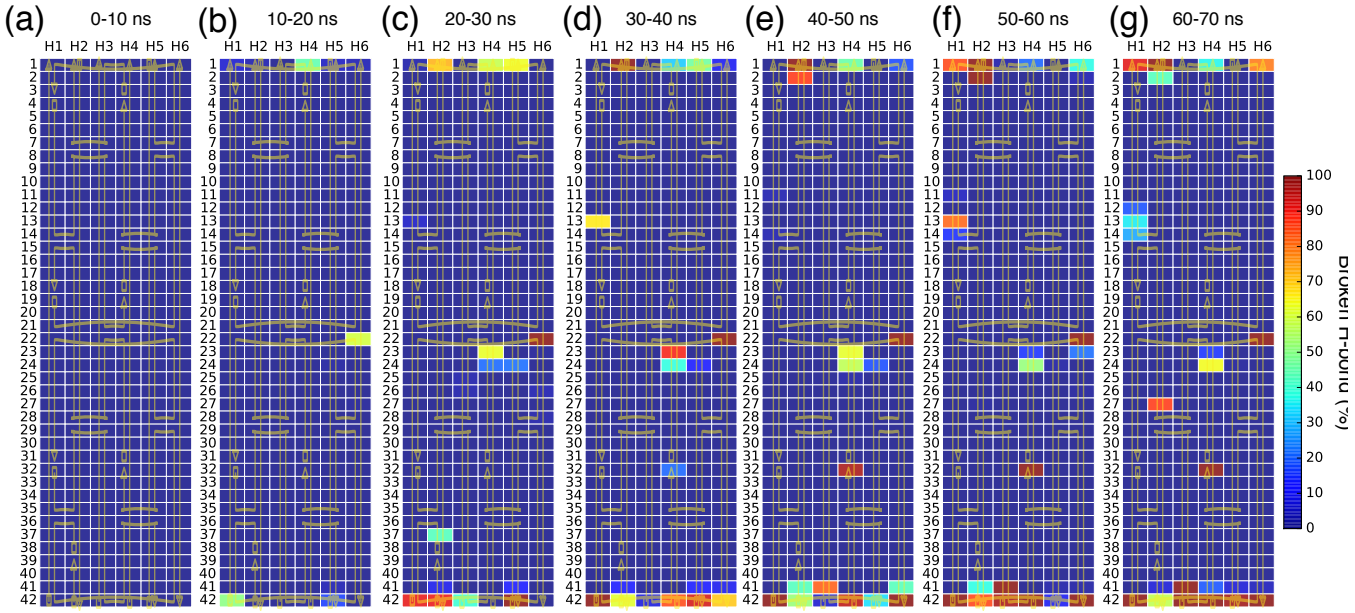

Figure S1: The probability of observing a broken basepair in System I for each of the seven 10-ns segments of the 70-ns equilibration trajectory. Each block corresponds to an individual basepair of the DNA structure; the probability is color-coded in each block. The caDNAno design of the channel is overlaid in orange.

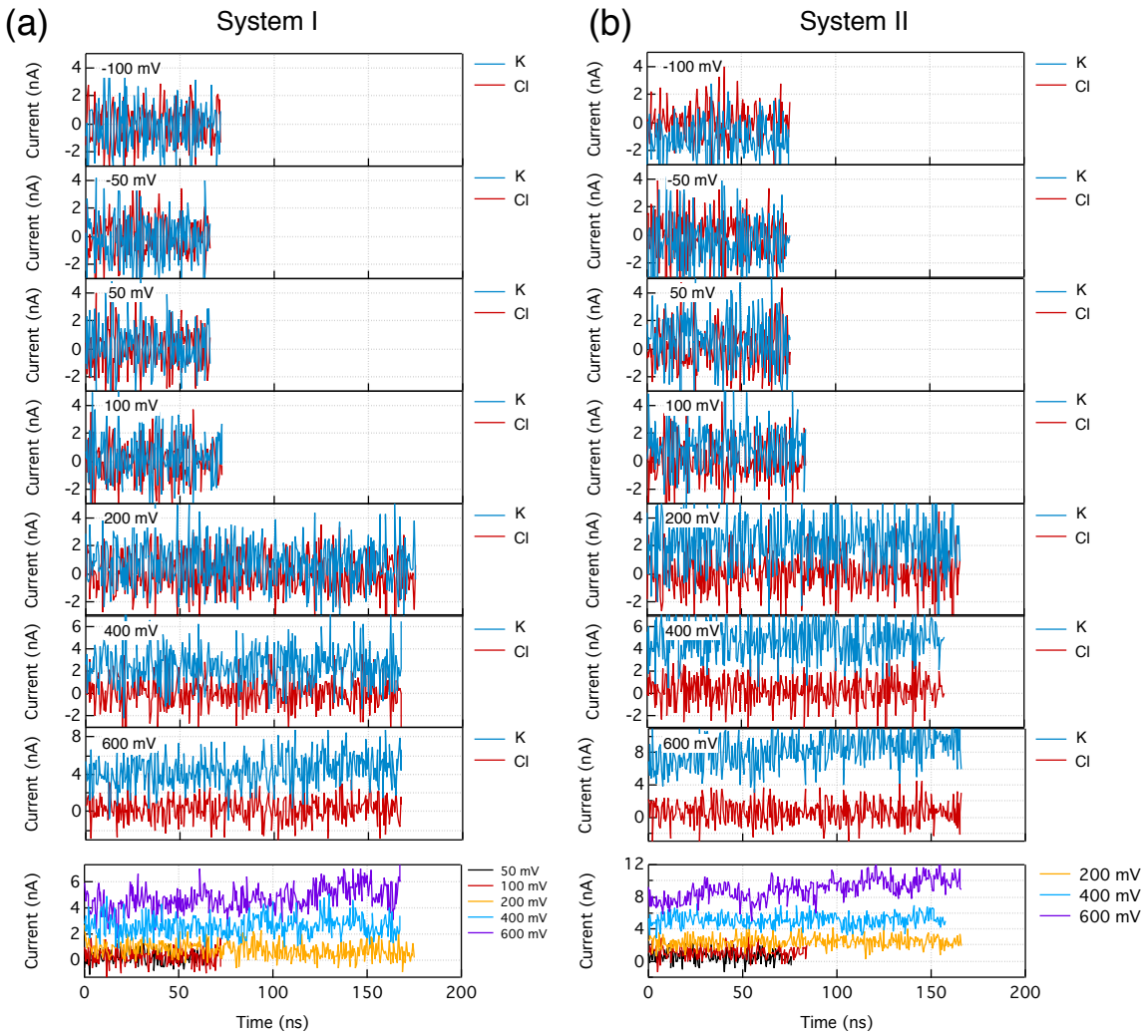

Figure S2: Simulated ionic current traces for System I (a) and System II (b) under zero tension conditions. (a) (Top seven rows) Ionic currents of K^+ (blue) and Cl^- (red) ions in System I as a function of time at a transmembrane bias of -100, -50, 50, 200, 400, and 600 mV. (Bottom row) Total ionic currents in System I at the seven voltages. (b) Same as in panel a but for System II. The currents were sampled every 4.8 ps, and 480-ps block averages are shown.

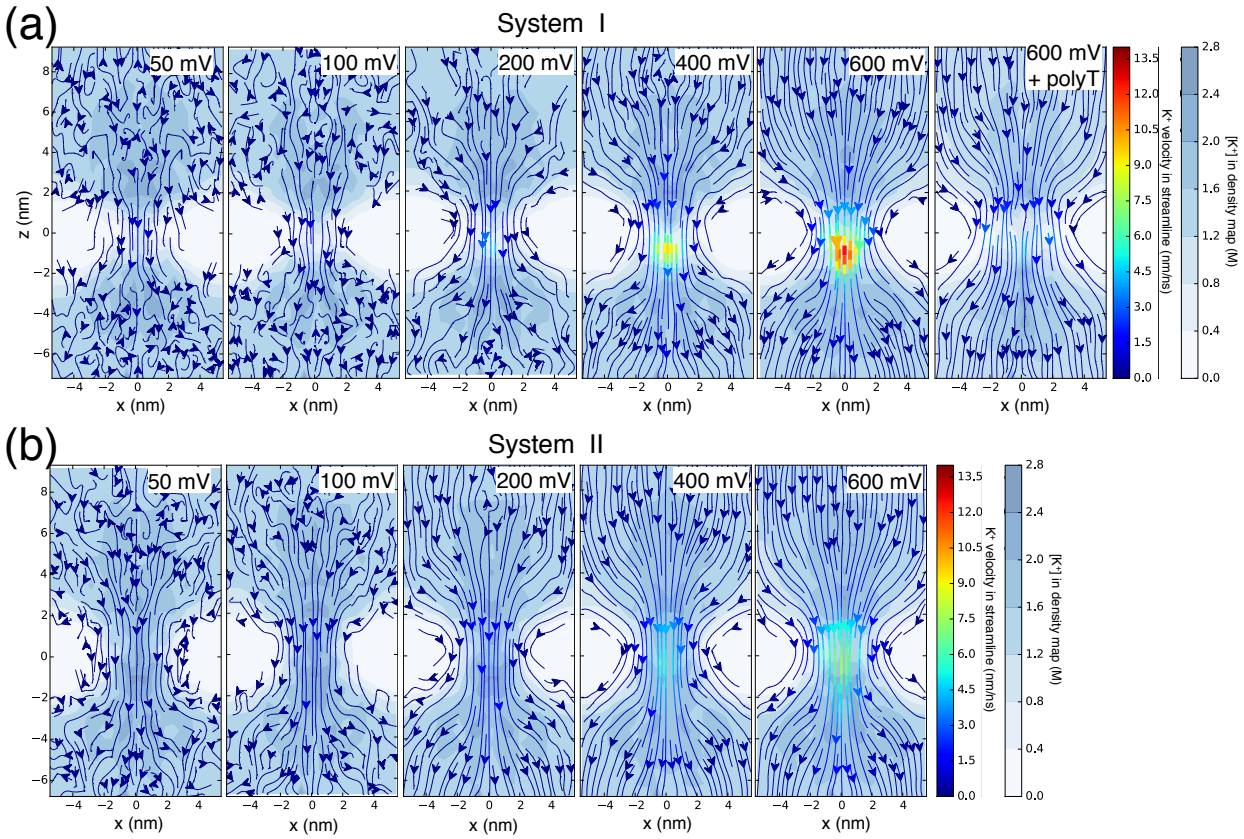

Figure S3: Density-flow maps of K^+ ions in System I (a) and System II (b). (a) (From left to right) Density-flow maps at 50, 100, 200, 400, 600 mV, and 600 mV with polyT ssDNA, respectively, in System I. (b) (From left to right) Density-flow maps at 50, 100, 200, 400, and 600 mV, respectively, in System II. Gray-scale map indicates the average local density of K^+. Color-coded streamline plots indicate the average local velocity of K^+.

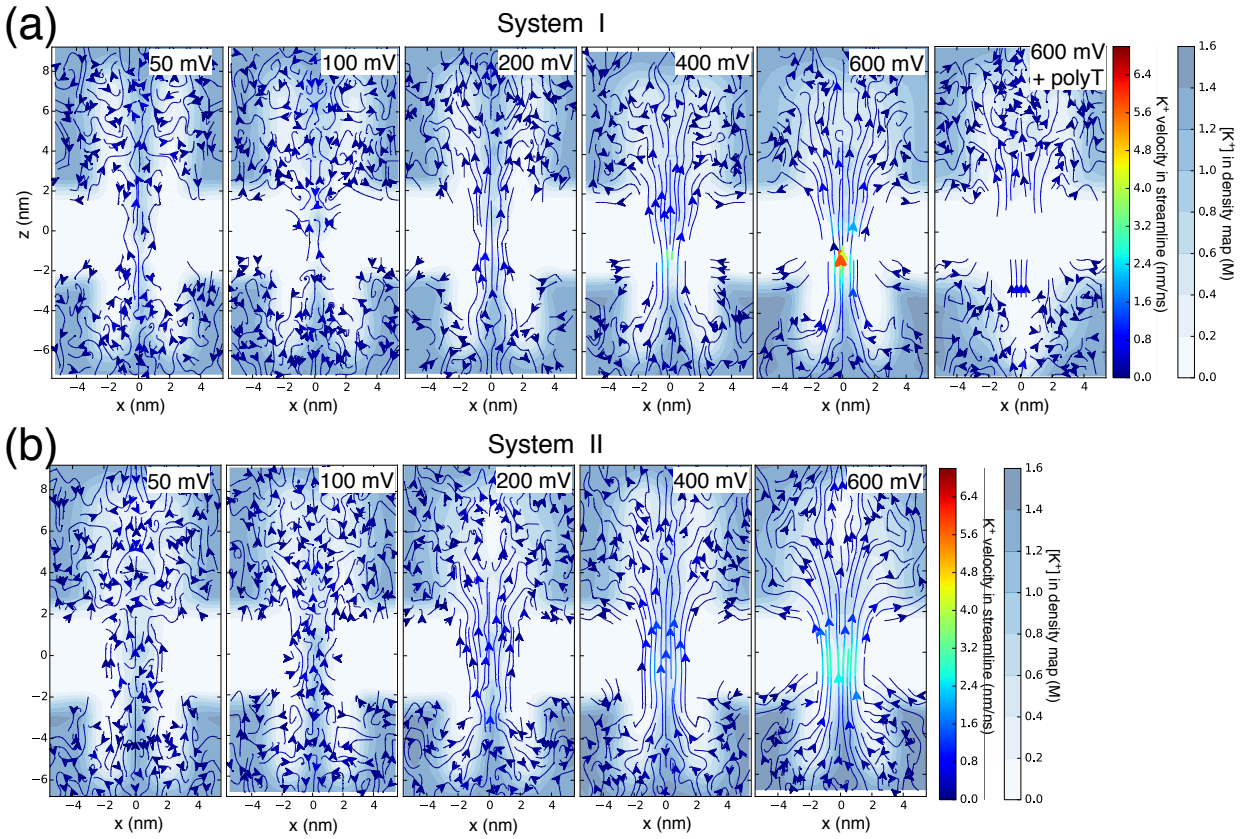

Figure S4: Density-flow maps of Cl^- ions in System I (a) and System II (b). (a) (From left to right) Density-flow maps at 50, 100, 200, 400, 600 mV, and 600 mV with polyT ssDNA, respectively, in System I. (b) (From left to right) Density-flow maps at 50, 100, 200, 400, and 600 mV, respectively, in System II. Gray-scale map indicates the average local density of Cl^-. Color-coded streamline plots indicate the average local velocity of Cl^-.

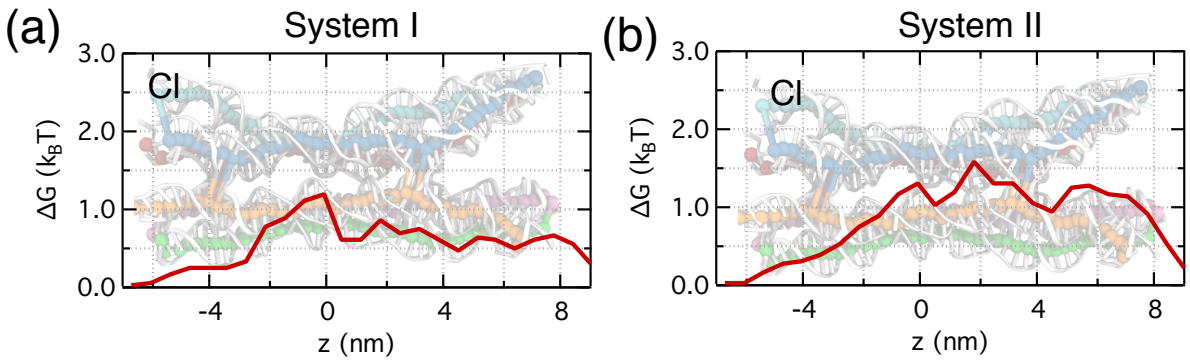

Figure S5: Free energy change (ΔG) of Cl^- ions along the channel axis. ΔG was computed by taking a Boltzmann inversion of the Cl^- concentration profile along the channel axis. The concentration profile was computed from the 150 ns production simulation of System I (a) and System II (b) by counting the number of ions in cylindrical bins of 1.0 nm radius and 0.7 nm spacing along the z axis.

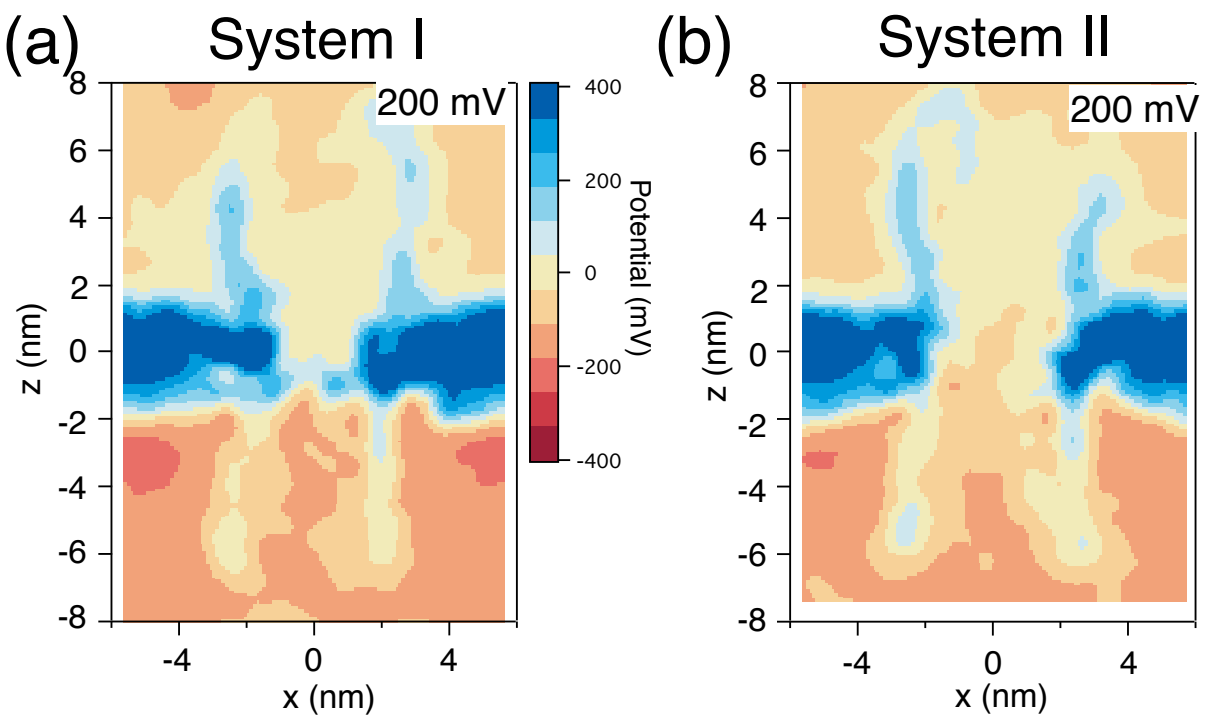

Figure S6: The distribution of the electrostatic potential in System I (a) and II (b) at a 200 mV transmembrane bias. 3D maps of the electrostatic potential were obtained by averaging the instantaneous distributions of the electrostatic potential[15] over the last 15 ns of the corresponding MD trajectory. The 2-D maps shown were obtained by averaging the corresponding 3-D maps over a 20-Å wide rectangular volume arranged parallel to the $x-z$ plane and centered at $y = 0$. The center of the transmembrane domain of the DNA channels are located at the origin.

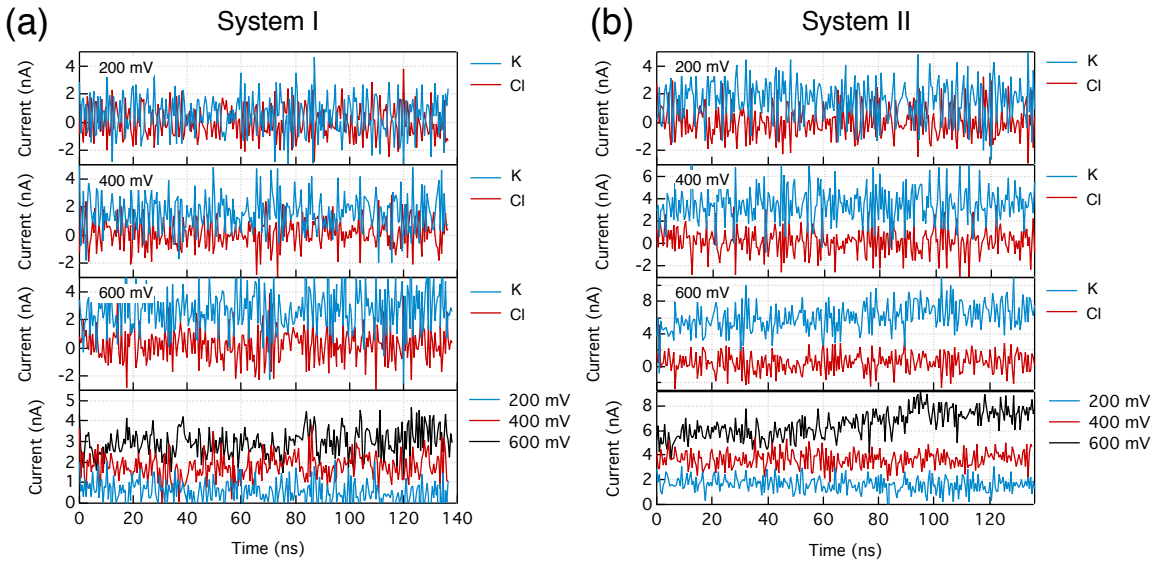

Figure S7: Ionic currents through System I (a) and System II (b) under the lipid compression conditions. (a) (Top three rows) Ionic currents of K^+ (blue) and Cl^- (red) in System I as a function of time at 200, 400, and 600 mV. (Bottom row) Total ionic currents in System I at the three voltages. (b) Same as in panel a but for System II. The currents were sampled every 4.8 ps, and 480-ps block averages are shown.

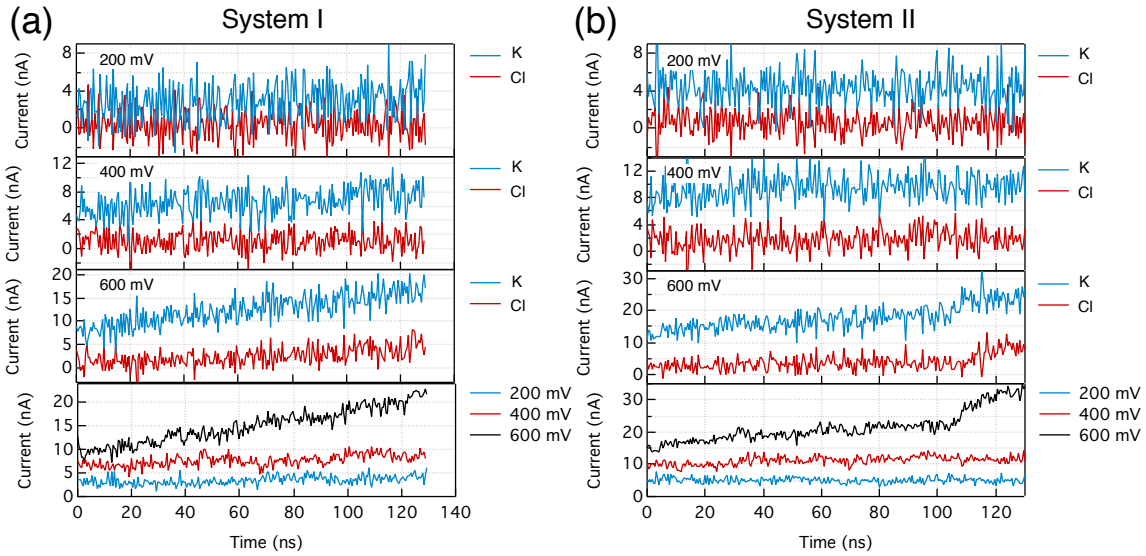

Figure S8: Ionic currents through System I (a) and System II (b) under the lipid extension conditions. (a) (Top three rows) Ionic currents of K^+ (blue) and Cl^- (red) in System I as a function of time at 200, 400, and 600 mV. (Bottom row) Total ionic currents in System I at the three voltages. (b) Same as in panel a but for System II. The currents were sampled every 4.8 ps, and 480-ps block averages are shown.

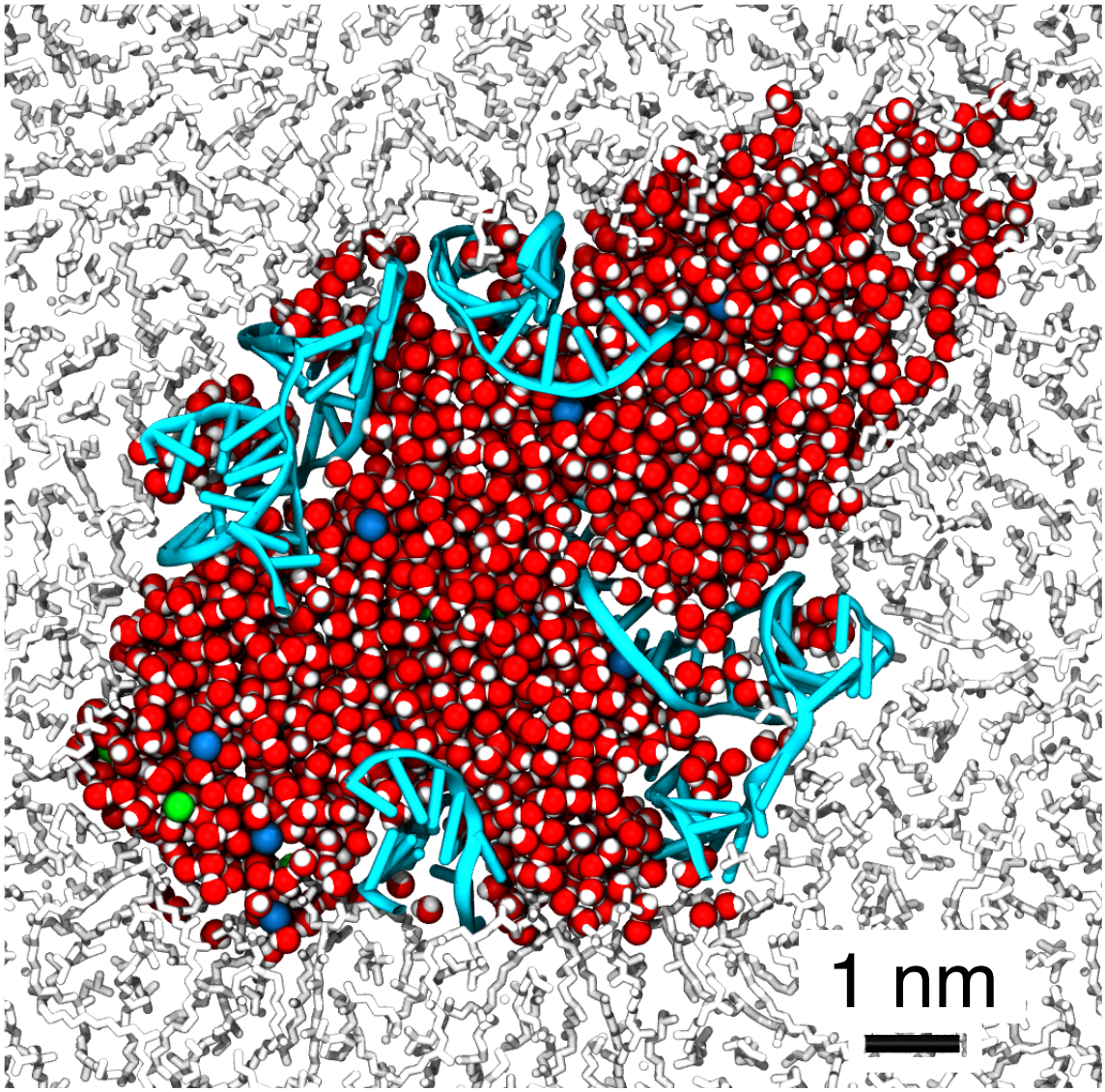

Figure S9: Rupture of the lipid-DNA interface at the end of the MD simulation of System I under the lipid extension conditions and a 600 mV transmembrane bias.

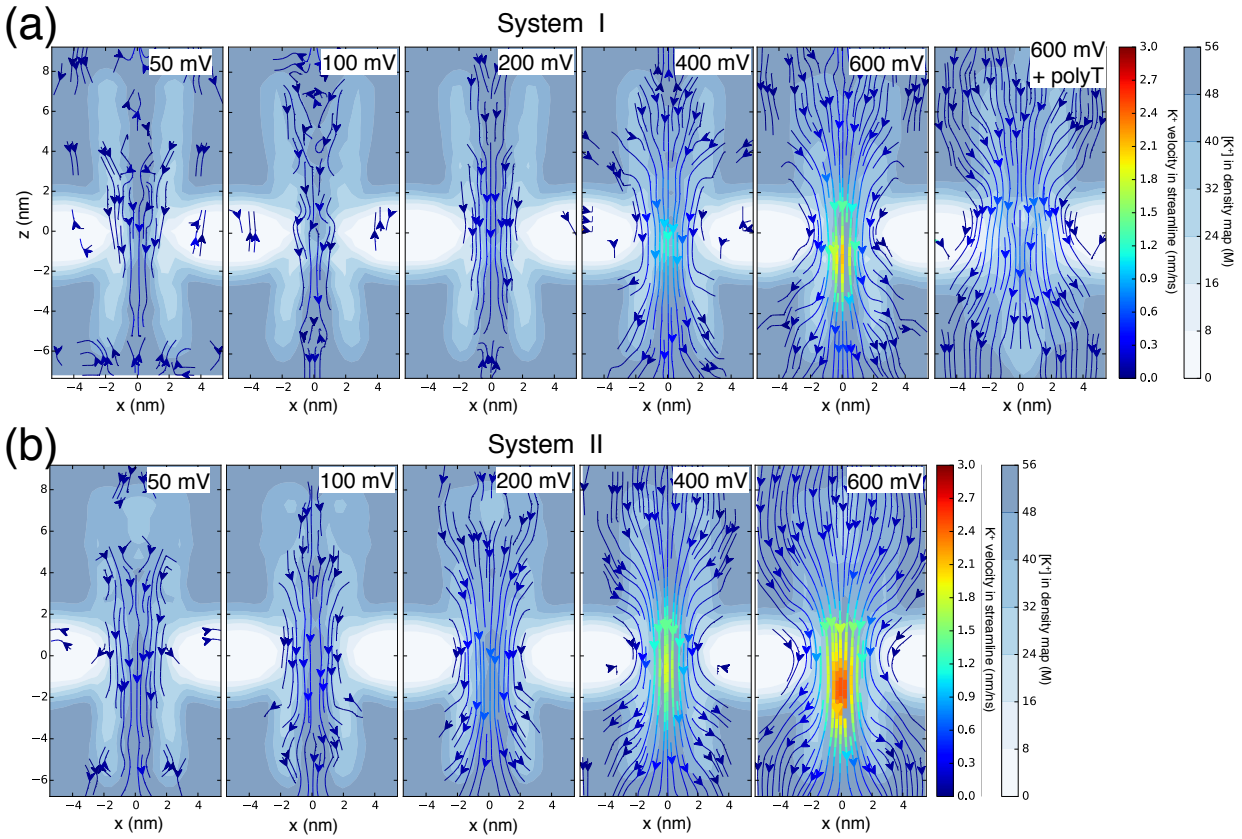

Figure S10: Density-flow maps of water in System I (a) and System II (b). (a) (From left to right) Density-flow maps at 50, 100, 200, 400, 600 mV, and 600 mV with polyT ssDNA, respectively, in System I. (b) (From left to right) Density-flow maps at 50, 100, 200, 400, and 600 mV, respectively, in System II. Gray-scale maps indicate the average local density of water. Color-coded streamline plots indicate the average local velocity of water.

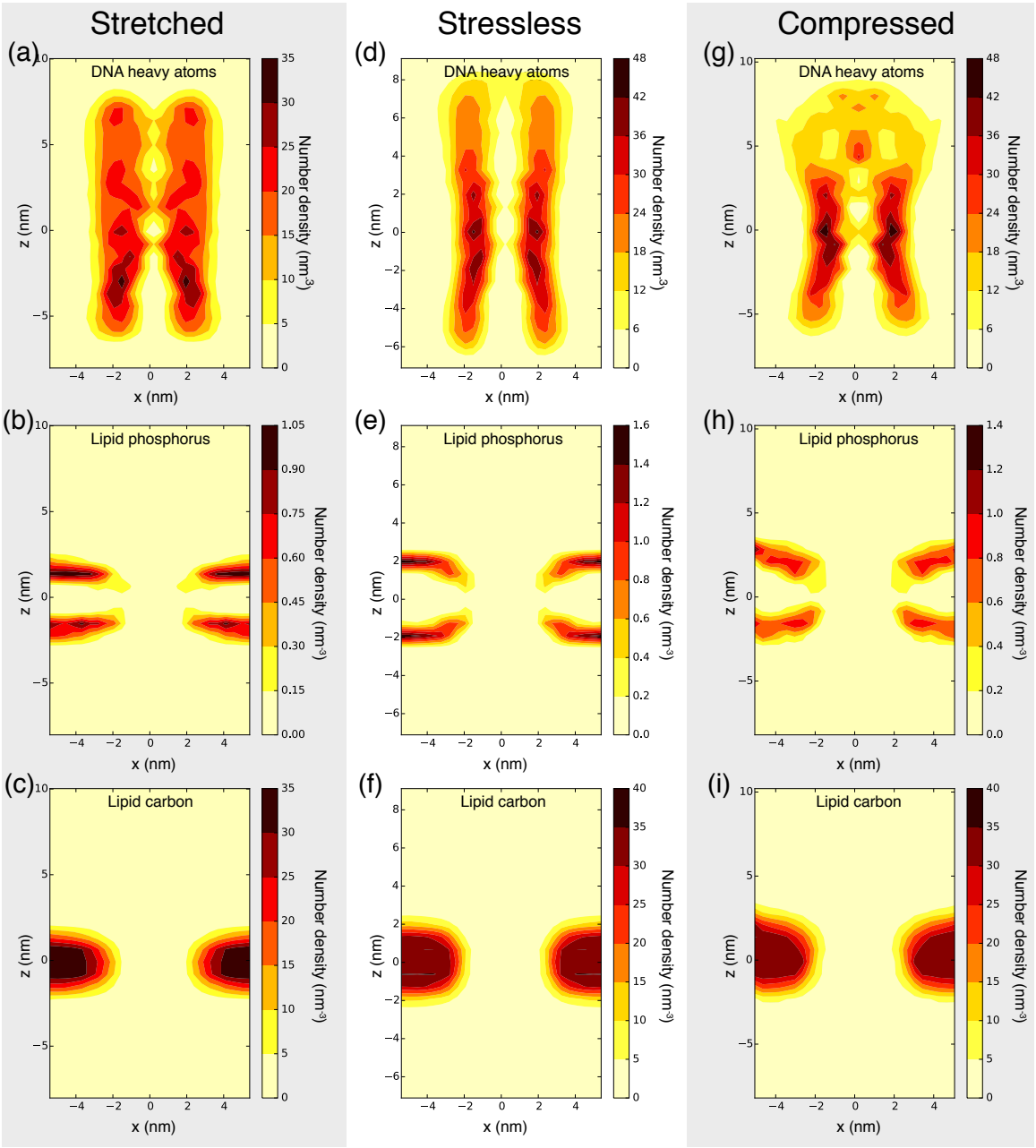

Figure S11: Spatial distributions of DNA and lipid atoms during the MD simulations of the stretched (a,b,c), stressless (d,e,f), and compressed (g,h,i) System I. Each map shows a cylindrical average of the respective 3D map. (a,b,c) Number density maps of DNA heavy atoms (a), lipid phosphorus (b), and lipid carbon atoms (c) for the stretched lipid bilayer membrane conditions. A mirror reflection of the map about the z axis is also shown for visual guidance. (d,e,f) Same plots as (a,b,c), respectively, but for the stressless simulation condition. (g,h,i) Same plots as (a,b,c), respectively, but for the compressed simulation condition.

Captions to movies

Movie 1. Internal structure of the DNA origami channel (System I) at the end of the 70-ns equilibration simulation. The DNA backbone and bases are shown in green and blue, respectively. Ethyl-modifications are shown with a vdW representation (carbon, cyan; hydrogen, white). Lipid molecules are shown with white molecular bonds.

Movie 2. Structural fluctuation of the DNA channel in System I during the last 13 ns of the 40 ns production simulation carried out in the absence of applied electric field or mechanical stress. Each DNA strand has a unique color. Lipid molecules are shown using a molecular bond representation (carbon, cyan; oxygen, red; nitrogen, blue; phosphorus, ochre).

Movie 3. Transmembrane transports of K^+ (blue spheres) and Cl^- (red spheres) ions through the pore of the DNA origami channel (System I) at a 600 mV transmembrane bias; the movie covers a 5 ns fragment of the MD trajectory. This simulation was carried out under the zero tension lipid bilayer condition. DNA is shown in gray, lipid and water molecules are not shown for clarity.

Movie 4. A typical trajectory of an ATP molecule that passes from one size of the membrane to the other through the transmembrane pore in System I. The ATP molecule is seen to move in the direction of the applied electric field (opposite to the direction prescribed by its negative charge). The movie covers a 300 ns MD trajectory. DNA backbone and bases are shown in green cartoon and blue molecular-bonds representations, respectively. An ATP molecule is shown in spheres colored by atom types: nitrogen, blue; oxygen, red; carbon, cyan; hydrogen, white. Lipid molecules are shown in gray molecular bonds.

References

(1) Phillips, J. C.; Braun, R.; Wang, W.; Gumbart, J.; Tajkhorshid, E.; Villa, E.; Chipot, C.; Skeel, R. D.; Kale, L.; Schulten, K. Scalable Molecular Dynamics with NAMD. *J. Comput. Chem.* **2005**, *26*, 1781–1802.

(2) Hart, K.; Foloppe, N.; Baker, C. M.; Denning, E. J.; Nilsson, L.; MacKerell, Jr., A. D. Optimization of the CHARMM Additive Force Field for DNA: Improved Treatment of the BI/BII Conformational Equilibrium. *J. Chem. Theory Comput.* **2012**, *8*, 348–362.

(3) Jorgensen, W. L.; Chandrasekhar, J.; Madura, J. D.; Impey, R. W.; Klein, M. L. Comparison of Simple Potential Functions for Simulating Liquid Water. *J. Chem. Phys.* **1983**, *79*, 926–935.

(4) Yoo, J.; Aksimentiev, A. Improved Parametrization of Li^+, Na^+, K^+, and Mg^{2+} Ions for All-Atom Molecular Dynamics Simulations of Nucleic Acid Systems. *J. Phys. Chem. Lett.* **2012**, *3*, 45–50.

(5) Yoo, J.; Aksimentiev, A. In situ structure and dynamics of DNA origami determined through molecular dynamics simulations. *Proc. Natl. Acad. Sci. U.S.A.* **2013**, *110*, 20099–20104.

(6) Vanommeslaeghe, K.; Hatcher, E.; Acharya, C.; Kundu, S.; Zhong, S.; Shim, J.; Darian, E.; Guvench, O.; Lopes, P.; Vorobyov, I. et al. CHARMM general force field: A force field for drug-like molecules compatible with the CHARMM all-atom additive biological force fields. *J. Comput. Chem.* **2010**, *31*, 671–690.

(7) Burns, J. R.; Stulz, E.; Howorka, S. Self-Assembled DNA Nanopores That Span Lipid Bilayers. *Nano Lett.* **2013**, *13*, 2351–2356.

(8) Lim, J. B.; Klauda, J. B. Lipid chain branching at the iso- and anteiso-positions in

complex Chlamydia membranes: a molecular dynamics study. *Biochim. Biophys. Acta* **2011**, *1808*, 323–31.

(9) Darden, T. A.; York, D.; Pedersen, L. Particle mesh Ewald: An N log(N) method for Ewald sums in large systems. *J. Chem. Phys.* **1993**, *98*, 10089–92.

(10) Martyna, G. J.; Tobias, D. J.; Klein, M. L. Constant pressure molecular dynamics algorithms. *J. Chem. Phys.* **1994**, *101*, 4177–4189.

(11) Douglas, S. M.; Marblestone, A. H.; Teerapittayanon, S.; Vazquez, A.; Church, G. M.; Shih, W. M. Rapid prototyping of 3D DNA-origami shapes with caDNAno. *Nucl. Acids Res.* **2009**, *37*, 5001–6.

(12) Yoo, J.; Sobh, A. N.; Li, C.-Y.; Aksimentiev, A. cadnano to PDB File Converter. `https://nanohub.org/tools/cadnanocvrt`.

(13) Brooks, B. R.; Brooks, C. L.; MacKerell, Jr., A. D.; Nilsson, L.; Petrella, R. J.; Roux, B.; Won, Y.; Archontis, G.; Bartels, C.; Boresch, S. et al. CHARMM: the biomolecular simulation program. *J. Comput. Chem.* **2009**, *30*, 1545–614.

(14) Li, C.-Y.; Hemmig, E. A.; Kong, J.; Yoo, J.; Hernández-Ainsa, S.; Keyser, U. F.; Aksimentiev, A. Ionic Conductivity, Structural Deformation and Programmable Anistropy of DNA Origami in Electric Field. *ACS Nano* **2015**, *9*, 1420–1433.

(15) Aksimentiev, A.; Schulten, K. Imaging α-Hemolysin with Molecular Dynamics: Ionic Conductance, Osmotic Permeability and the Electrostatic Potential Map. *Biophys. J.* **2005**, *88*, 3745–3761.